Creating corners in kitchen sinks

When a vertical jet of liquid from a nozzle hits a flat surface, as in tap water striking the kitchen sink, a discontinuity appears in a ring created by the flow. At this deformation the depth of the water alters abruptly (the 'circular hydraulic jump'[1–5]) at some distance from the jet. We have now discovered that if the jet contains a liquid more viscous than water, stationary polygonal patterns form, breaking axial symmetry. The sharp corners of the polygons carry a large radial flux, while the sides generate resistance to the stream.

To account for the appearance of these remarkable structures in a simple flow, we followed a classic idea[1] to design the experiment shown in Fig. 1a. Close to the jet, the fluid layer is thin (of height h_{int}) and the motion is rapid, whereas further away the layer height is increased by an order of magnitude to h_{ext} and the fluid moves correspondingly more slowly.

The transition between these two types of motion occurs within a surprisingly short distance — a millimeter or so. The horizontal surface was a large disc (diameter 36 cm) made of glass so that the jump can be observed from below. The fluid going over the rim around the disc is collected and recirculated, and the rim can be raised or lowered to control h_{ext} (ref. 4).

The circular jump can occur in two states that have different cross-sectional flow patterns. When h_{ext} is small, we observe a type I pattern, in which the surface velocity is outward everywhere and a separation bubble is present at the bottom just outside the jump. On increasing h_{ext}, the jump becomes steeper, until, at a critical value of h_{ext}, fluid outside the jump flows inwards and breaks over the edge of the jump[4].

When a new steady state (type II pattern) is reached, a surface eddy has formed. This eddy, called a 'roller' or a 'surfing wave', has the geometry of a floating torus surrounding the jump (Fig. 1a). The outgoing flow passes under the roller. This maintains the rotation of the roller and an inward surface velocity near the jump.

In experiments with ethylene glycol (antifreeze), which is about ten times more viscous than water, the circular type II state (Fig. 1b) frequently undergoes spontaneous breaking of its azimuthal symmetry into a stationary polygonal shape (Fig. 1c). Rather than displaying the weak angular deformations generally seen in fluids, the jumps form clear corners and edges that are often straight (Fig.1c,d) but which can curve outwards or inwards.

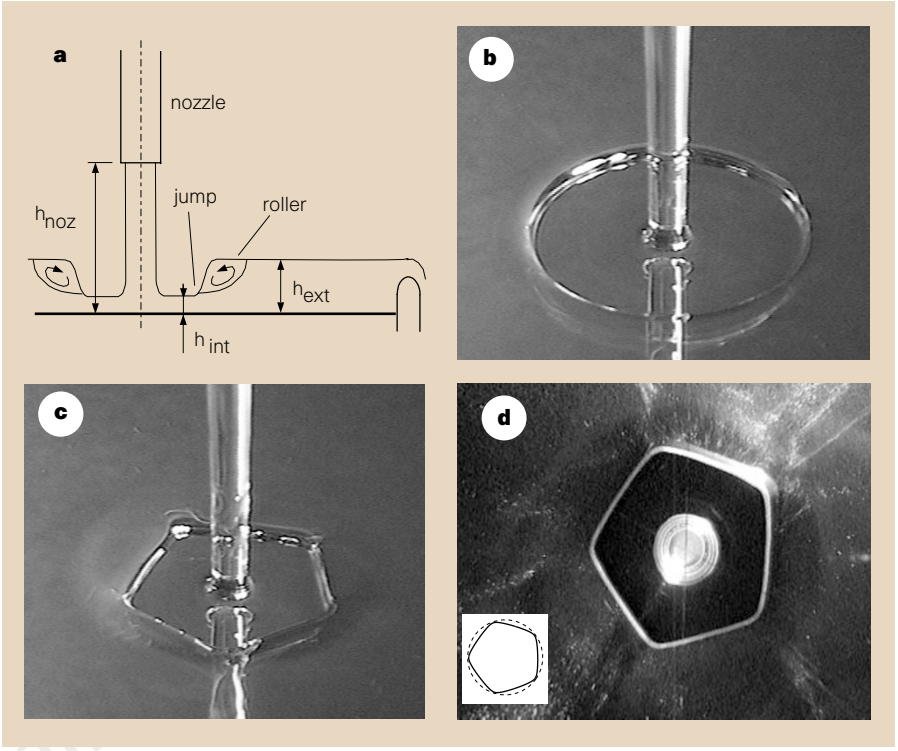

Figure 1 The hydraulic jump experiment. A cross-sectional flow structure (type II pattern) is shown in **a**; **b–d** are video images of three stationary states. The fluid is ethylene glycol (antifreeze; about 99% pure) and typical flow rates, Q, are 30–50 ml s^{-1}. The external height, h_{ext}, is increased from **b** to **c**, causing the familiar circular jump in **b** to change spontaneously to polygons with many corners (not shown), then to a pentagon (**c**), viewed from underneath in **d**. In **d**, the bright circle in the centre is the vertical jet; the corners of the surrounding polygonal jump are clearly evident. The inset shows one solution to our model.

These states are robust — they reappear if the flow is temporarily disrupted or scrambled. However, several polygon states can be stable for the same h_{ext}.

There is an interval of h_{ext} in which, for example, a pentagon can be deformed into a hexagon through provoking another corner by locally dragging a side of the jump with a pin. Corners prefer to be equally spaced: if not, a drift and an adjustment in the azimuthal direction occurs over a long period (sometimes lasting for hours), even though the radial flow is rapid.

As h_{ext} is raised from the type I configuration, the wave breaking may create many corners: polygons with up to 14 corners are created by changing the flow rate Q, the height of the nozzle outlet h_{noz}, and the kinematic viscosity n. As h_{ext} is increased further, the corners disappear, usually one by one, and the circumference of the jump becomes smaller until the jump eventually 'closes'.

There is a considerable hysteresis effect in the sense that several polygons can be stable at the same flow parameters. Interestingly, all these coexisting polygons seem to have exactly the same corner shape.

Inside the roller, a slow spiralling flow develops towards the corner, where the roller breaks up.

How can such unusual structures occur in these simple flows? We have derived a model which assumes that radial forces on the roller, namely the hydrostatic inward pressure and the outward shear force from the radial flux, balance at any angle, even when the radial flux is allowed to vary. This balance results in a relation between the width of the roller and the radial flux at a given angle.

If we further assume that the roller possesses a weak line tension, and therefore that the shape chosen is the one with minimal circumference for a given imposed flux, we get a simple variational problem that can be solved numerically (one of the computed shapes is shown in Fig.1d). The model can be treated as non-dimensional so that the only parameter is the dimensionless flux ϕ, which equals $\nu Q/(g(h_{ext}^2 - h_{int}^2)^2)$.

The circular jump exists for all values of ϕ, and more corners arrive as it increases. There is overlap of the intervals of ϕ for which various polygons exist, so that several polygons can be found for the same system

parameters, just as we find in the experiments described here.

Clive Ellegaard, Adam Espe Hansen, Anders Haaning, Kim Hansen, Anders Marcussen, Tomas Bohr, Jonas Lundbek Hansen, Shinya Watanabe
Center for Chaos and Turbulence Studies, The Niels Bohr Institute, Blegdamsvej 17, DK-2100 Copenhagen, Denmark

1. Rayleigh, Lord *Proc.Roy.Soc.Lond. A* **90,** 324–328 (1914).
2. Craik, A., Latham, R., Fawkes, R. & Gribbon, P. *J. Fluid Mech.* **112,** 347–362 (1981).
3. Bohr, T., Dimon, P. & Putkaradze, V. *J.Fluid Mech.* **254,** 635–648 (1993).
4. Bohr, T., Ellegaard, C., Hansen, A. E. & Haaning, A. *Physica B* **228,** 1–10 (1996).
5. Bohr, T., Putkaradze, V. & Watanabe, S. *Phys. Rev. Lett.* **79,** 1038–1041 (1997).

Electron microscopy image enhanced

One of the biggest obstacles in improving the resolution of the electron microscope has always been the blurring of the image caused by lens aberrations. Here we report a solution to this problem for a medium-voltage electron microscope which gives a stunning enhancement of image quality.

Even today, more than 60 years after the invention of the transmission electron microscope[1], the point resolution is still limited by the spherical aberration of its objective lens. Up until now, the only way to improve matters was to impose a numerical correction for this spherical aberration that was based either on a series of images of the object taken under variable objective-focus conditions[2] or on the application of holographic techniques[3].

Fifty years ago, Scherzer[4] suggested that the two principal axial aberrations, chromatic and spherical, could be corrected by electrostatic or magnetic multipole elements, but this proved to be beyond the technology available at that time. Our solution for spherical aberration correction derives from a much more recent suggestion by Rose[5], and depends on two electromagnetic hexapoles and four additional lenses.

The principle by which correction is achieved is based on the fact that the primary aberrations of second order from the first hexapole are compensated by the second hexapole element. However, the two hexapoles additionally induce a residual secondary third-order spherical aberration which is rotationally symmetric[6] and proportional to the square of the hexapole strength.

The appertaining coefficient of spherical aberration is of the opposite sign to that of the objective lens. In this way, the spherical aberration of the entire system can be compensated by exciting the hexapoles appropriately[7].

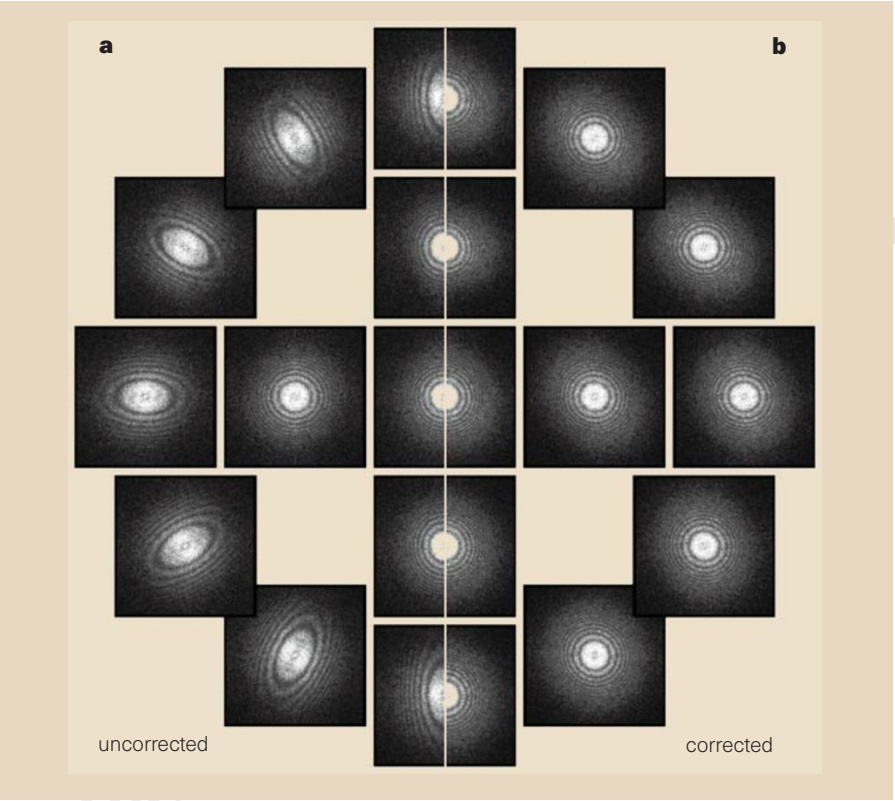

Figure 1 Diffractogram tableau of the microscope. **a,** Uncorrected, and **b,** after correction for spherical aberration and proper alignment. The beam tilt angle is 10.8 mrad in both cases and the azimuthal angles vary between 0 and 2π in steps of $\pi/6$. The essentially identical shape of the diffractograms in **b** indicates the vanishing spherical aberration.

In the transmission electron microscope, off-axial aberrations are as important as axial ones. Therefore, in order to maintain a finite field of view, a semi-aplanatic objective lens system had to be constructed which fulfils Abbe's sine condition. This means that it is not only free of spherical aberration but also of off-axial coma and parasitic axial aberrations resulting from misalignment of the optical system.

Spherical aberration correction is not enough to improve the resolution of the microscope. It is necessary to compensate as well for the parasitic second-order axial aberrations, coma and threefold astigmatism, and adequately to suppress the non-spherical axial third-order aberrations, star aberration and fourfold astigmatism. For this purpose, the aberration coefficients are determined by means of an extended version of the diffractogram tableau method[8].

With the corrector switched off, a diffractogram tableau of an amorphous sample is recorded digitally (Fig. 1a) and evaluated on-line in terms of induced defocus and twofold astigmatism. Switching on the corrector introduces misalignment aberrations and an appropriate alignment procedure has to be carried out; this semi-automatic alignment takes about 15 minutes.

The diffractogram tableau of the corrected and aligned system is shown in Fig. 1b. All diffractograms are of roughly the same shape, indicating the properties

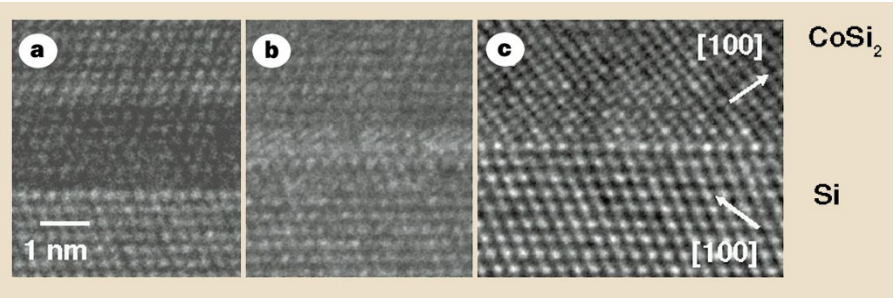

Figure 2 Structure images of an epitaxial Si(111) $CoSi_2$ interface demonstrating the production of image artefacts by the effect of contrast delocalization due to spherical aberration. Images in **a** and **b** were taken in the uncorrected microscope at Scherzer defocus and Lichte defocus, respectively. **c,** Image taken in the aberration-corrected state at Scherzer defocus does not show any delocalization (C_s = 0.05 mm).